Effect of Wave Radiation Stress in Storm Surge-Induced Inundation: A Case Study for the East Coast of India

P. L. N. Murty,[1] A. D. Rao,[2] K. Siva Srinivas,[1] E. Pattabhi Rama Rao,[1] and Prasad K. Bhaskaran[3]

Abstract—Tropical cyclone-induced coastal inundation is a potential hazard for the east coast of India. In the present study, two case studies are presented to examine the significance and importance of wave radiation stress in storm surge modeling during two extreme weather events associated with the Phailin and Hudhud cyclones. Model computations were performed using the advanced circulation (ADCIRC) model and the coupled ADCIRC + SWAN (Simulating Waves Nearshore) model for these two events. Meteorological and astronomical forcing were used to simulate the hydrodynamic fields using the ADCIRC model run in a stand-alone mode, whereas the coupled ADCIRC + SWAN model also incorporated the wave radiation stress attributed from wave breaking effects. Cyclonic wind fields were generated using the revised Holland model. Results clearly indicate an increase in the peak surge of almost 20–30% by incorporating the wave radiation stress and resulting inundation scenario in the coupled model simulation. The validation exercise showed that the coupled ADCIRC + SWAN model performed better than the ADCIRC model in stand-alone mode. Key findings from the study indicate the importance of wave-induced setup due to radiation stress gradients and also the role of the coupled model in accurately simulating storm surge and associated coastal inundation, especially along flat-bottom topography.

Keywords: Wave radiation stress, coupled model, storm surge, inundation extent, ADCIRC + SWAN, unstructured mesh.

1. Introduction

The east coast of India (ECI) is characterized by a highly productive estuarine environment, mangrove ecosystem and thickly populated coastal cities. Low-lying coastal areas along the ECI are highly susceptible and vulnerable to the impact of storm surges due to landfalling tropical cyclones that originate in the Bay of Bengal basin. The national weather agency has categorized both *Phailin* and *Hudhud* cyclones as very severe cyclonic storms (VSCS) that made landfall along the ECI near Gopalpur, Odisha and Visakhapatnam, Andhra Pradesh, respectively. These two VSCS resulted in a trail of destruction during landfall, thereby causing widespread damage to infrastructure, property and a few instances of loss of human life in the coastal regions of Odisha and northeastern Andhra Pradesh. Coastal flooding or inundation is a catastrophe having significant impact on any coastal zone, causing loss of life and property and widespread damage to coastal infrastructure. Timely warnings of storm surge and inundation forecasts during cyclones can potentially reduce the loss of life by issuing bulletins and alerts to stakeholders. Numerical modeling of coastal inundation during cyclonic events is a vital element in issuing warnings for emergency planning and evacuation measures. While several studies had focused on storm surge modeling along the ECI (Murty et al. 1986; Dube et al. 1997, 2000; Rao et al. 1994), very few studies have focused on modeling inundation scenarios during storm surge events. Rao et al. (2012) investigated coastal inundation scenarios along the ECI attributed due to tropical cyclones. Bhaskaran et al. (2014) performed a detailed analysis on the potential of coastal inundation at several coastal locations off Tamil Nadu. A study by Srinivasa et al. (2015) investigated the possible worst-case scenario by considering the combination of highest high water levels with storm surge that generates huge

[1] Earth System Science Organisation (ESSO), Indian National Centre for Ocean Information Services (INCOIS), Hyderabad 500 090, India. E-mail: murty.pln@incois.gov.in; murtypln.incois@gmail.com

[2] Centre for Atmospheric Sciences, Indian Institute of Technology (IIT), Hauz Khas, New Delhi 110 016, India.

[3] Department of Ocean Engineering and Naval Architecture, Indian Institute of Technology Kharagpur, Kharagpur 721 302, West Bengal, India.

devastation during cyclones. Their study highlights the importance of the tidal phase and its relevance in controlling the extent of inland inundation during tropical cyclone landfall.

In a shallow-water environment, storm surge and wind waves can interact with each other by transferring energy from one system to the other. It is well known that wind waves can ultimately affect the coastal ocean circulation by enhancing the wind stress (Mastenbroek et al. 1993). Surface waves constitute sea surface roughness, and for a strong wind regime such as in tropical cyclones (> 30 m/s), they tend to decrease the surface drag (Hwang 2018) when other important processes start to play an important role (e.g. sea spray). The study by Hwang (2018) also indicates that both surface roughness and whitecaps due to wave breaking are driven by surface wind stress, and their quantification using the wind speed input depends on the drag coefficient formulation. A previous study by Rajesh et al. (2009) attempted to develop a parameterization of sea surface drag under varying sea states dependent on wave age. Their study (Rajesh et al. 2009) combined the Toba-3/2 power law and Froude number scaling to develop a new drag formulation found to perform well under conditions of both young and mature waves, verified against time series meteorological and oceanographic observations in the Indian Ocean region. Usually, these physical processes can influence one another in numerous ways: wind stress that is altered by including the wave effect (Donelan et al. 1993); wave radiation stress considered to be an additional forcing term in storm surge models (Xie et al. 2001; Mellor 2003; Xie et al. 2004). The concept of radiation stress was first introduced by Longuet-Higgins and Stewart (1962) to analyze the mechanism of wave setup and set-down in a nearshore environment.

In shallow waters, storm surges, tides and wind waves are the major components in an ocean forecasting system that determines the sea-state environment of that region. It is known that these processes are present in many cases and their interactions are very significant in context to individual dynamic processes (Longuet-Higgins and Stewart 1960; Prandle and Wolf 1978; Janssen 1992; Bao et al. 2000; Welsh et al. 2000). Wind waves play a significant role in determining the sea surface roughness that in turn affects the currents in coastal circulation models (Smith et al. 1992). Although short- and long-period waves are separated in a wave spectrum, they interact. Breaking waves in shallow water generate radiation stress gradients that in turn drive wave setup and currents affecting the vertical momentum mixing, bottom friction and the resultant water level elevations. According to the conservation of wave energy flux, the wave height and steepness have a tendency to increase as they propagate into shallow water environments. The shallow-water wave process is dominated by depth-induced breaking, wherein momentum flux is transferred to the water column, raising the water levels adjacent to the coast (Holthuijsen 2007). The dynamic characteristics of water level elevation and wave-induced setup and set-down along coastal areas, especially during an approaching storm, have cumulative effects that depend on the mutual interaction between waves, currents, surge and the astronomical tides. In fact, tidal propagation is also modified in the presence of a surge, leading to tide-surge interaction (Horsburgh and Wilson 2007), and the waves are modified by the presence of currents generated by the tide and surge. They contribute to resultant water level and mean circulation through wave-induced setup and currents, attributed to radiation stresses created by breaking waves in shallow water (Longuet-Higgins and Stewart 1962). The dynamic interaction between wave–current–surge–tide components and their combined energy balance is very strong during tropical cyclone activity. Hence, the nonlinear interaction mechanism and the influence of waves on coastal currents and storm surge has been an important area of research area in recent years. The key question lies in how these nonlinear processes can be properly accounted for and coupled in numerical models.

Application of coupled wave hydrodynamic models for the global ocean is a recent development that has been observed in a few studies such as the MAST III PROMISE Project (Ozer et al. 2000); the modeling of energetic events such as hurricane Katrina and Rita in 2005, and Gustav and Ike in 2008 in the Atlantic Ocean (Dietrich 2010); modeling of the Mediterranean Sea with focus on the Italian coast (Ferrarin et al. 2013); and a coupled modeling system for typhoon Maemi in Korean seas (Bung et al. 2013).

Arora and Bhaskaran (2012) reported on the importance of bottom friction under combined wave-tide action and its relevance to bottom boundary layer characteristics (Arora et al. 2010). The role of wave-induced setup during an extreme event for the Kalpakkam coast (Nayak et al. 2012) and associated coastal vulnerability was studied by Nayak and Bhaskaran (2013). A few studies have emphasized the importance of coupling storm surges, waves and tides to enhance the accuracy of storm surge forecasts in coastal areas (Roland et al. 2009; Brown and Wolf 2009; Wolf 2009). During severe cyclones, in particular, radiation stress-induced wave setup is an important component which needs to be included in a storm surge model, as it can account for significant increase in water level along the coast (Brown et al. 2011). Araújo et al. (2011) studied the importance of including wave setup along the Viana do Castelo (Portugal) coast. A more recent study by Murty et al. (2014) and Murty et al. (2016) highlighted the significance of including wave setup in computing surge heights along the Odisha coast and for the West Bengal coast (Gayathri et al. 2016). However, their study does not investigate the effect of wave setup on inundation extent. Therefore, in the present study, the effect of wave setup on inundation extent is examined using a coupled wave and hydrodynamic model. The coupled model was used to study the characteristics of wave setup and inundation extent associated with two VSCS, the Phailin and Hudhud cyclones. The objective is to understand the effect of wave–current interaction on storm surges and inundation mutually transferred through wave radiation stress in storm surge computation.

2. Modeling System

The ADCIRC hydrodynamic model and coupled ADCIRC + SWAN model are used in the present study. Cyclonic wind fields were derived using the Holland dynamic wind model (Holland et al. 2010).

2.1. Wave Model: SWAN

The wind-wave model, Simulating Waves Nearshore (SWAN), was used to predict the evolution of surface gravity waves in time and geographic space. It computes the wave direction (θ) and relative frequency (σ) based on the action balance equation (Booij et al. 1999), as given below:

$$\frac{\partial}{\partial t}N + \frac{\partial}{\partial x}c_x N + \frac{\partial}{\partial y}c_y N + \frac{\partial}{\partial \sigma}c_\sigma N + \frac{\partial}{\partial \theta}c_\theta N = \frac{S}{\sigma} \quad (1)$$

where N represents the wave action density; S is the source term (combination of source and sinks) in terms of energy density; c_θ is the propagation velocity in θ space; c_σ is the propagation velocity in σ space; c_x and c_y are the respective propagation velocities along the x and y directions. The first, second and third terms on the left-hand side of Eq. (1) represent the rate of change of wave action in time and the propagation of wave action in geographic space, respectively. The current study used the unstructured SWAN model (version 40.85) coupled with a surge hydrodynamic model (ADCIRC). SWAN computes the wave action density spectrum at the unstructured mesh nodes by using a sweeping algorithm and updates the action density using information from the adjacent nodes. A detailed description of the SWAN model is available in Booij et al. (1999). In the current study the unstructured version of SWAN (UNSWAN) is used that implements an analog to the four direction Gausse–Seidel iteration method supplying unconditional stability (Zijlema, 2010).

2.2. Surge Hydrodynamic Model: ADCIRC

The advanced circulation (ADCIRC) model, developed at the University of North Carolina, is a multidimensional, depth-integrated, barotropic time-dependent long-wave finite-element hydrodynamic circulation model. The model can be run either as a two-dimensional depth-integrated (2DDI) or as a three-dimensional (3D) model. Both the vertically integrated (ADCIRC-2DDI) and the fully 3D (ADCIRC-3D) models solve the vertically integrated continuity equation for water surface elevation. A detailed description of ADCIRC is given in Luettich et al. (1992).

In the current study, the ADCIRC-2DDI version is used for the simulations. In the baroclinic version of ADCIRC-3D, the bottom boundary friction layer of

surface Ekman wind will be better resolved as compared with the ADCIRC-2DDI (barotropic) version. However, as the radiation stress induced by breaking waves is confined to very shallow and nearshore waters, the use of ADCIRC-2DDI in the current study can be justified. However, for a detailed study on wave–current interaction in intermediate water depths, it would be better to study the simulation performed using the ADCIRC-3D model.

2.3. Coupling Methodology

The ADCIRC and SWAN models run on the same local unstructured mesh, and are coupled by passing mutual information from each other (Dietrich et al. 2011). Due to the sweeping method incorporated in the SWAN model, it usually larger time steps than the ADCIRC model (Dietrich et al. 2011).

ADCIRC runs first within the coupling interval and then passes the currents, water levels and wind velocity to SWAN during the prescribed coupled run. Complete details of the coupling procedure between the SWAN and ADCIRC models used in the present study are available in Dietrich et al. (2011). Using the wave radiation stress information from SWAN, water levels and the currents from ADCIRC are revised and thus mutually exchanged with SWAN to further update the radiation stress. The radiation stress gradient (τ_s) computed by the SWAN model is expressed in the form:

$$\left.\begin{aligned}\tau_{sx,\text{wave}} &= -\frac{\partial S_{xx}}{\partial x} - \frac{\partial S_{xy}}{\partial y} \\ \tau_{sy,\text{wave}} &= -\frac{\partial S_{xy}}{\partial x} - \frac{\partial S_{yy}}{\partial y}\end{aligned}\right\} \quad (2)$$

where S_{xx}, S_{xy} and S_{yy} are the wave radiation stresses.

The two models march ahead in time by forcing each other by mutually exchanging the information. Figure 1 provides more details on the basic coupling algorithm between the SWAN and ADCIRC models.

2.4. Atmospheric Forcing

Surface wind stress and pressure gradients are the key driving forces for the computation of storm surges (Rao et al. 2012). Surface wind stress acts in parallel and pressure gradient in a direction normal to
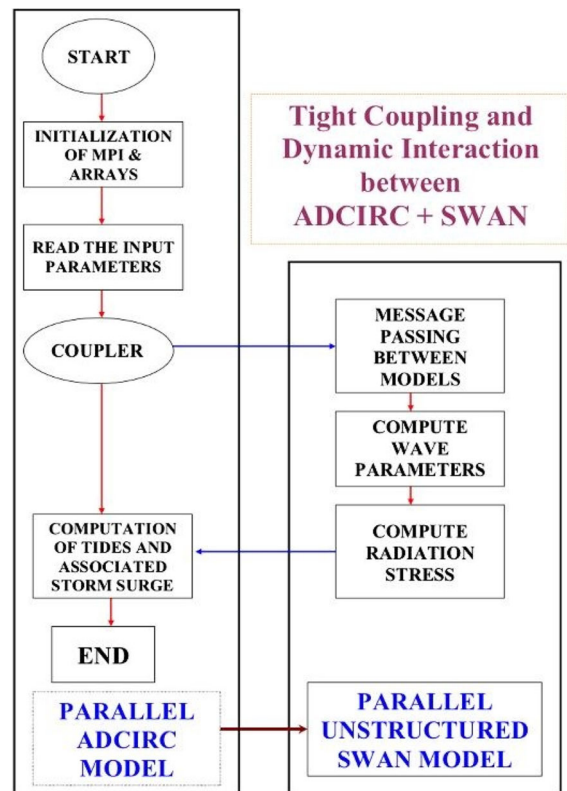

Figure 1
Basic structure of the ADCIRC + SWAN coupling system

the sea surface, and their relative significance depends on the water depth. Parametric wind models and the winds from global numerical weather hindcast/forecast models are commonly used for storm surge and wave computations. Global/mesoscale models are not available at a high resolution in forecast mode to provide realistic cyclonic wind fields. Even robust meteorological nowcasts have preprocessing delays pertaining to huge input datasets (Fleming et al. 2008). In addition, the demand of computational resources is required to address the mesoscale and synoptic-scale convection processes in operational weather models, which limit their use as a regular operational forecast of hurricane winds (Smita and Rao 2018). On the contrary, parametric cyclonic wind models are easier to use, and they produce improved wind fields with desired spatial resolution for storm surge simulations (Houston et al. 1999). In this context, a dynamic wind model (Holland et al. 2010; hereafter referred to as H10) is used in the present study. H10 is the revised

version of an earlier model (Holland 1980; hereafter referred to as H80). The H10 has several advantages over the earlier formulations, including (a) enhanced ability to contain both external and core wind observations; (b) less dependence on precise knowledge pertaining to radius of maximum wind, R_{max}; (c) capability to handle bimodal wind profiles connected with secondary eye wall production; and (d) abridged matters with lack of resolution in some cyclones in the proximity of R_{max}, which can lead to underrating the true maximum winds, or overrating external winds if the core is artificially improved (H80) (Holland et al. 2010).

Surface wind speed can be computed radially using the mathematical formulation:

$$v_s = \left[\frac{100 b_s \Delta p_s \left(\frac{r_{v_m}}{r}\right)^{b_s}}{\rho_s e^{\left(\frac{r_{v_m}}{r}\right)^{b_s}}} \right]^x \text{ or } \tag{3}$$

$$v_s = v_m \left\{ \left(\frac{r_{v_m}}{r}\right)^{b_s} e^{\left[1 - \left(\frac{r_{v_m}}{r}\right)^{b_s}\right]} \right\}^x \tag{4}$$

where v_s is the radial surface wind speed, v_m is the maximum wind speed, b_s is a scaling parameter, x is a shape parameter, r_{v_m} is the radius of maximum winds and r is the radial distance from the center.

b_s, x and v_m values can be calculated as

$$b_s = -4.4 \times 10^{-5} \Delta p_s^2 + 0.01 \Delta p_s + 0.03 \frac{\partial p_{cs}}{\partial t} - 0.014 \varphi + 0.15 v_t^x + 1.0, \tag{5}$$

$$x = 0.6 \left(1 - \frac{\Delta p_s}{215}\right), \tag{6}$$

$$v_m = \left(\frac{100 b_s}{\rho_{ms}} \Delta p_s\right)^{0.5} \tag{7}$$

where Δp_s in hPa, $\frac{\partial p_{cs}}{\partial t}$ is the rate change of intensity in hPa/h, φ is the latitude in degrees and v_t is the cyclone translation speed in m/s.

The surface air density can be derived as:

$$\rho_s = \frac{100 p_s}{R T_{vs}}, \tag{8}$$

$$T_{vs} = (T_s + 273.15)(1 + 0.61 q_s), \tag{9}$$

$$q_s = RH_s \left(\frac{3.802}{100 p_s}\right)^{e^{\frac{17.67 T_s}{243.5 + T_s}}}, \text{ and} \tag{10}$$

$$T_s = \text{SST} - 1, \tag{11}$$

where $R = 286.9 \text{ J Kg}^{-1}$ represents the gas constant for dry air, T_{vs} is the virtual surface temperature (in K), q_s is the surface moisture (in g Kg^{-1}), T_s and SST are the surface temperature and sea surface temperature (both in °C), respectively, and RH_s is the surface relative humidity (assumed at 0.9 in the absence of direct observations). Detailed description and formulation is available in Holland et al. (2010).

3. Methodology

SMS (surface water modeling system) software is used to generate the unstructured triangular mesh used in the present study. General Bathymetric Chart of the Ocean (GEBCO) 30-arc second data is used as inland topography and ocean bathymetry owing to its high resolution. The generated mesh comprises 1,089,458 elements and 547,927 nodes. The mesh resolution varies from 100 m in the nearshore regions to about 30 km in the deeper waters. This selection of grid spacing is based on the study by Blain et al. (1998) and Rao et al. (2009). Their studies propose that a nearshore mesh resolution of 250 m or less is sufficient to represent the peak surge during cyclones. Along the landward boundary, the 15-m height contour is taken as a rigid boundary in order to compute the horizontal extent of inundation from the coastline, assuming that the storm surge height does not exceeded 15 m. Model mesh and bathymetry used for Hudhud and Phailin simulations are shown in Fig. 2a. Figure 2b, c shows the magnified view of the mesh around Konada (Andhra Pradesh) and Ganjam (Odisha) locations, respectively, in order to have a clear picture of fine grid spacing representing the coastal regions. The Le Provost tidal database (Le Provost et al. 1998) was used to prescribe the tidal constituents along the open ocean boundary. The 13 tidal constituents (K1, O1, P1, Q1, M2, N2, S2, L2, K2, T2, 2N2, NU2 and MU2) are provided along the open ocean boundary. The model was initially forced with the above-mentioned tidal constituents for a
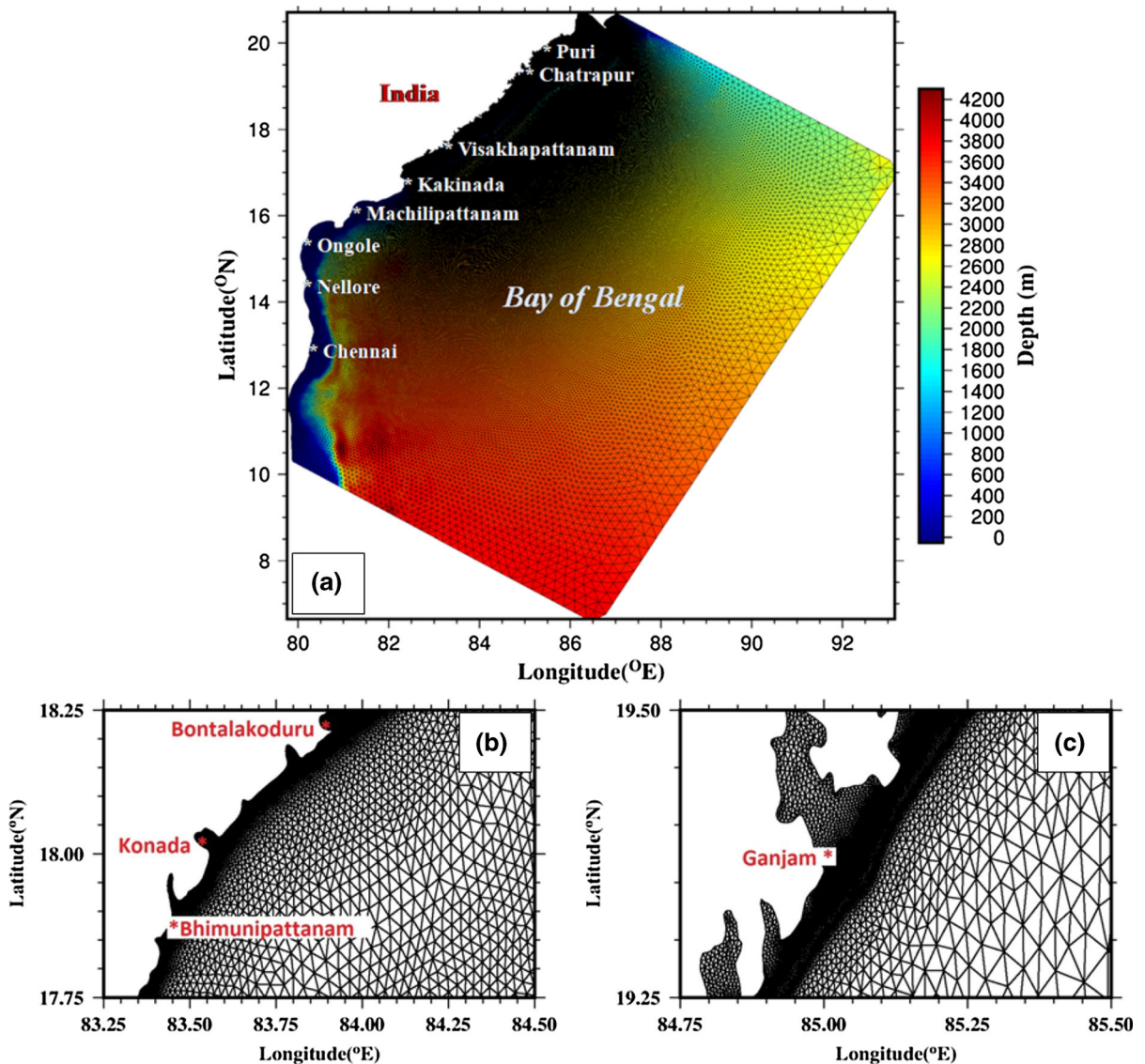
Figure 2

a Model mesh that shows the domain and bathymetry; **b** enlarged portion of the mesh showing the enhanced grid resolution in shallow waters around the Konada, Andhra Pradesh, region; **c** enlarged portion of the mesh showing the enhanced grid resolution in shallow waters around the Ganjam, Odisha, region

period of 61 days initiating with a cold start to establish steady-state conditions. Thereafter, the model-computed cold-start information was subsequently provided for model runs in a hot-start mode that additionally considers the wind forcing. The computed tide is also validated at Visakhapatnam and Paradip locations to ensure that the model performed well in simulating the water levels. A comparison of

the water levels from the model against in situ observations at Visakhapattanam and Paradip locations is shown in the top and bottom panels of Fig. 3, respectively, which indicates a very good match. Both ADCIRC (in stand-alone mode) and coupled ADCIRC + SWAN models are used for simulations in the present study. The bottom friction coefficient was taken as 0.0028 (Zachry et al. 2013; Ziegler et al.
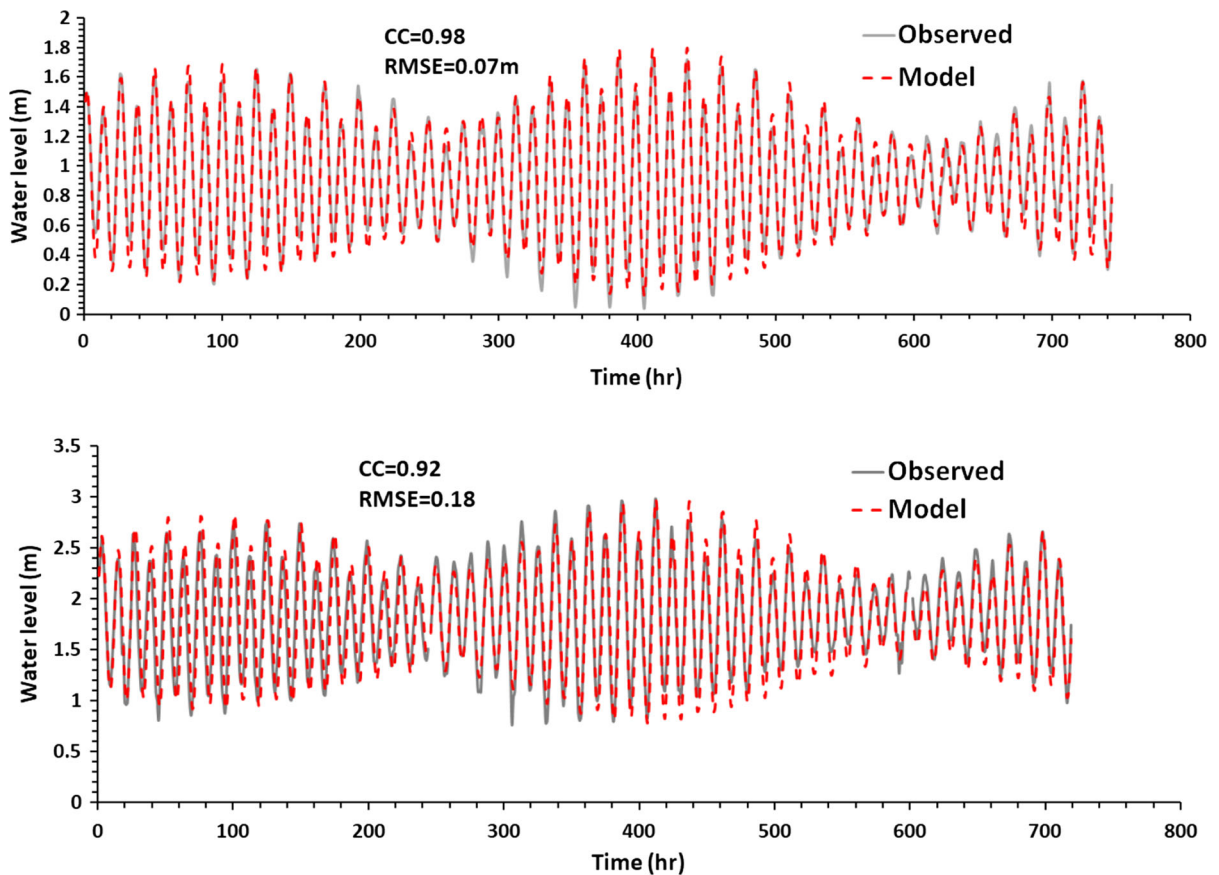
Figure 3
Validation of modeled tide at Visakhapattanam (upper panel) and at Paradip (lower panel)

1993; Vongvisessomjai and Rojanakamthorn 1989), and the model time step prescribed as 4 s. The coupling time interval and SWAN time step were set to 600 s (Bhaskaran et al. 2013) which could capture well the nonlinear interaction effects arising due to currents and water level changes on the resultant wave field. The SWAN model is implemented in a non-stationary mode prescribed with 34 frequency bins and 36 directional bins. The frequency bins range between 0.04 and 1.0 Hz, and the wave direction has an angular resolution of 10°. Nonlinear wave–wave interaction in the deep water based on Hasselmann et al. (1985) is employed in the SWAN model. The bottom friction formulation used in the SWAN model is based on Madsen et al. (1988) which allows for the spatially varying roughness length. The constant quadratic bottom friction coefficient used in

the study for both the coupled and uncoupled model is 0.0028 (Vongvisessomjai and Rojanakamthorn 1989; Ziegler et al. 1993; Zachry et al. 2013). The bottom friction coefficient selected in this study is best suited for the sandy bottom environment along the Andhra coast, an optimum configuration with both ADCIRC and SWAN models (Murty et al. 2014). However, the variable bottom friction option over the ocean and flooded/dried areas can further enhance the results. The primary and main forcing for the storm surge model is the cyclonic wind stress. In the present study, the wind and pressure fields are derived from the revised Holland dynamic wind model (Holland et al. 2010). The current version of ADCIRC used in the study applies the wind drag coefficient from Garratt (1977); SWAN applies a nearly identical wind drag coefficient from Wu

(1982). The SWAN + ADCIRC model limits the wind drag coefficient to a maximum of 0.002. The wind drag can be better represented by considering the Powell sector-based wind drag formulation (Powell and Reinhold 2007). However, this will be the scope of a future study. Snapshots of the spatial wind field during the landfall time of Hudhud and Phailin are shown in Fig. 4a, b, respectively. The model-computed water level elevations, significant wave height, and inundation extents are also validated against the available field observations.

4. Results and Discussion

The ADCIRC model run in stand-alone mode considers the astronomical tidal forcing along the open-ocean boundary along with wind forcing, whereas the coupled ADCIRC + SWAN model also considers additional forcing due to the wave radiation stress. As the tide–surge interaction is quite significant in a shallow-water environment, the astronomical tide forcing forms an integral component and, therefore, must be included in the surge computations instead of linearly superposing the water level elevation after carrying out the storm surge computations. Owing to the importance of tide in altering the resultant water level/total water

elevation (i.e., total water level obtained due to combined "surge and tide" from ADCIRC simulation and due to "surge, tide and wave" from coupled ADCIRC + SWAN simulation), the tidal component is included in the model simulations. However, the surge residual is also computed by removing the astronomical component from the resultant water level to evaluate the resultant water level changes solely attributed due to the wind forcing. The significance of a wave-induced setup in storm surge inundation modeling is examined based on simulations carried out for recent severe cyclones Hudhud and Phailin.

4.1. Cyclone Hudhud

Hudhud was an extremely severe cyclonic storm that made landfall near Visakhapatnam, ECI, on 12 October 2014 and also considered as the most intense cyclone that made landfall at this location during the last two decades. The track details of Hudhud cyclone are shown in Fig. 5. Model simulation (both coupled and uncoupled) was performed for 96 h. The H10-computed maximum wind speed was around 52 m/s (as shown in Fig. 4a) which is in close agreement to the IMD-reported value of 51 m/s (Kotal et al. 2015).
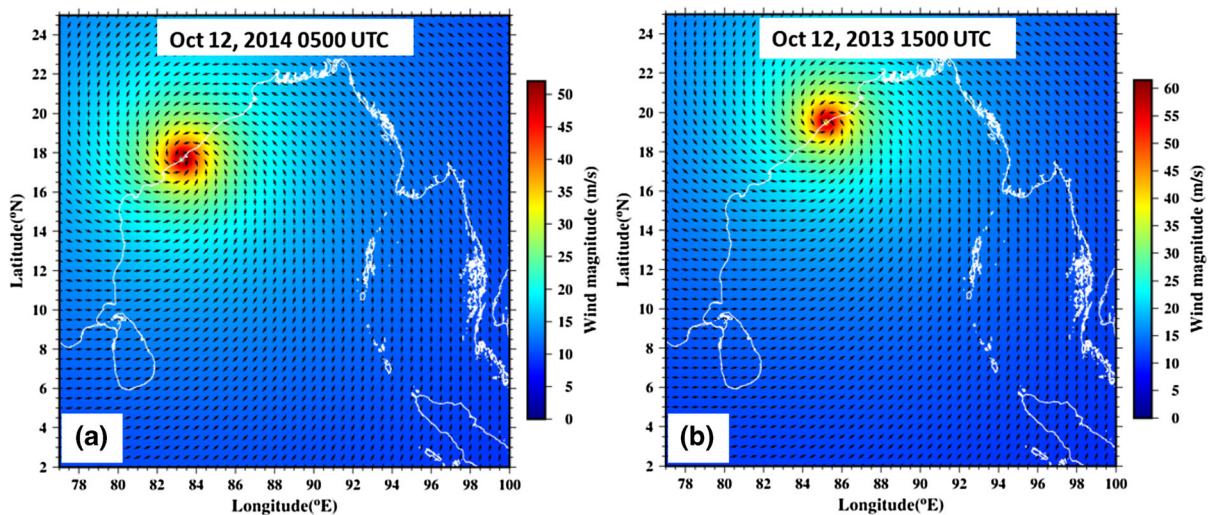

Figure 4
Snapshot of spatial wind field during landfall of **a** Hudhud and **b** Phailin cyclones
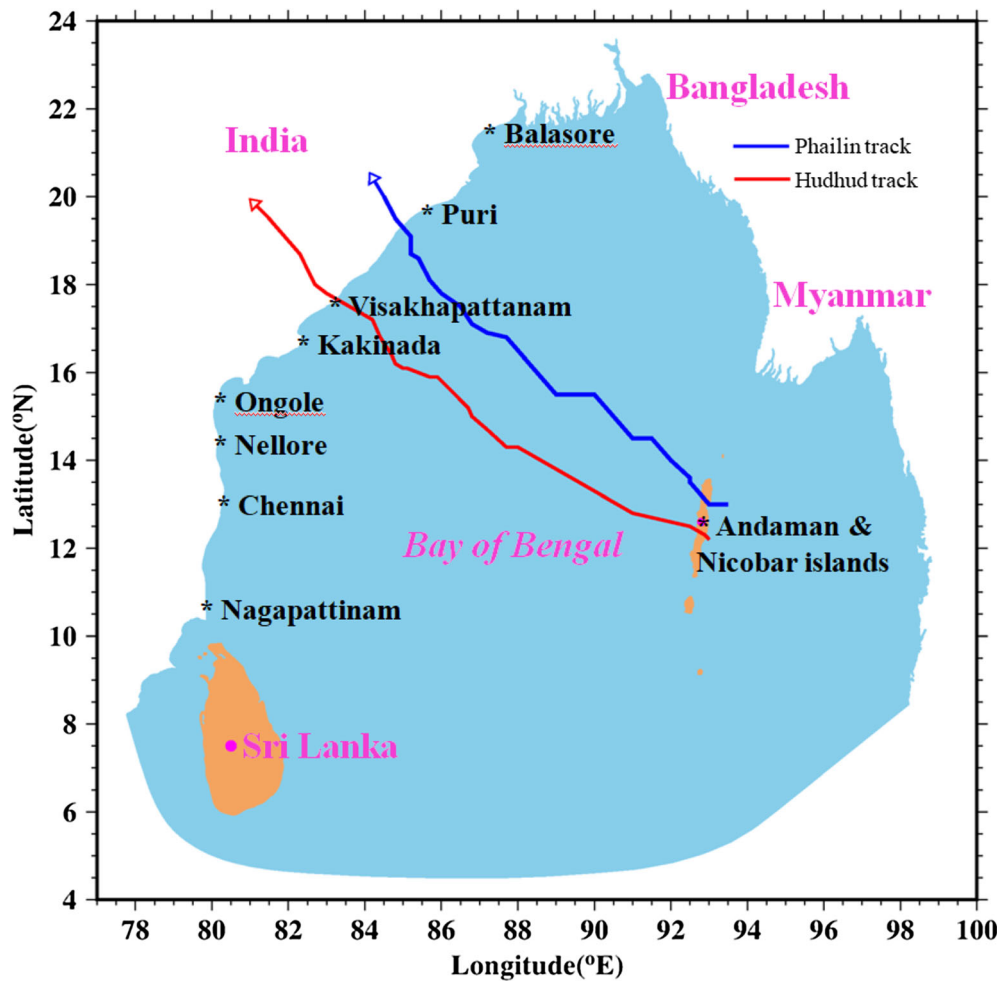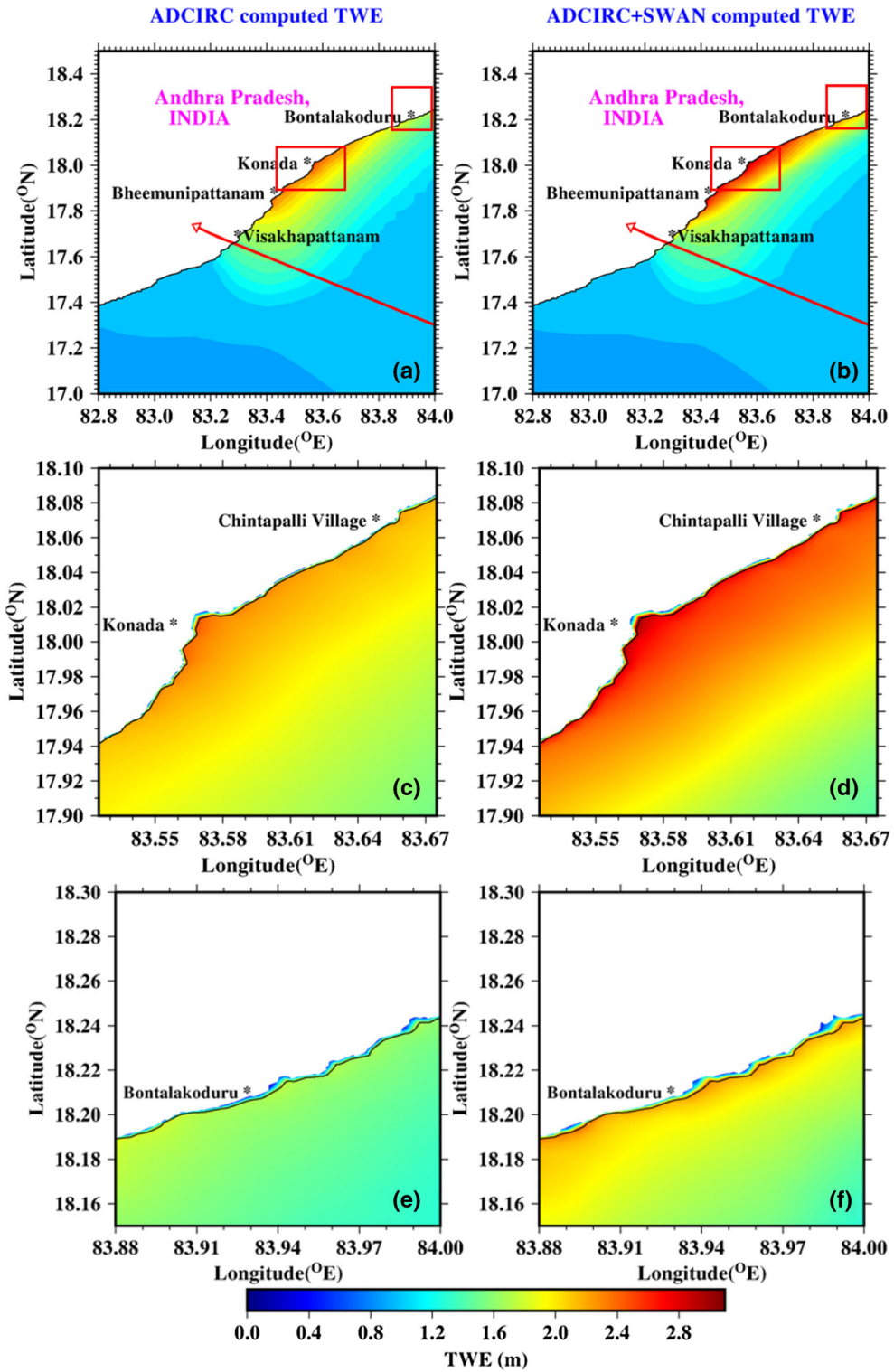
Figure 5
Tracks of Hudhud and Phailin cyclones

Storm surge simulations were carried out using the ADCIRC stand-alone and coupled ADCIRC + SWAN models. In both these simulations, the computed peak surge was observed near Konada (83.57°E, 18.01°N), Vijayanagaram district. The uncoupled run showed a peak storm surge of about 2.4 m, whereas that for the coupled model run was about 3.0 m. Spatial representation of the total water elevation (hereafter TWE) and inundation extents computed by the uncoupled and coupled models are shown in Fig. 6a, b respectively. Figure 6c, d shows the magnified version seen in Fig. 6a, b, respectively, at the Konada location. Similarly, Fig. 6e, f shows the magnified versions corresponding to Fig. 6a, b,

respectively, at Bontalakoduru (83.93°E, 18.21°N) location. It is very clear that the computed TWE and inundation extents from coupled runs are higher than those from the uncoupled runs. The maximum difference observed in the TWE between uncoupled and coupled model runs is about 0.6 m. This clearly demonstrates that the wave radiation stress in the coupled simulation contributes about a 20% increase in the resultant TWE. Spatial distribution of wave-induced water levels is shown in Fig. 7, which is the difference between TWEs from uncoupled and coupled model runs. Figure 7 clearly shows that the coastal stretch from the landfall point spanning up to Srikakulam is strongly influenced by wave-induced

◀Figure 6

Spatial depiction of storm surge levels and computed inundation extents due to Hudhud by **a** uncoupled and **b** coupled runs. **c** Enlarged view of red-colored box in **a** at the Konada location, **d** enlarged view of red-colored box in **b** at the Konada location, **e** enlarged view of red-colored box in **a** at the Bontalakoduru location and **f** enlarged view of red-colored box in **b** at the Bontalakoduru location. (TWE is the acronym for total water elevation, and red arrows indicate the cyclone track)

setup, with a peak value of 0.6 m corresponding to Cyclone Hudhud. Table 1 provides more details on the assessment of TWEs and inundation extent (with and without wave-induced setup) at different locations resulting from Hudhud landfall. The nearest available tide gauge station for validation of the computed surge residuals is located at Visakhapatnam (83.28°E, 17.68°N). A comparison of the computed TWE and surge residuals against measured data off Visakhapatnam is shown in Fig. 9a, b

respectively. The comparison demonstrates a very good match between model computation and observation data. In addition, it is clear from Fig. 9b that the primary and secondary peaks of surge maxima are very well represented by the model, as seen in observations deciphering the fact that the modeled wind fields are realistic in estimating storm surge. Figure 9c and d illustrates the time evolution of TWE and surge residuals, respectively, at the location of peak surge (Konada) during Hudhud. The arrow mark shown in figure indicates the landfall time of Hudhud. As there was no observation available at the peak surge location, only the modeled TWE and surge residuals are shown in Fig. 9c, d, respectively. As seen from the figure, there is only a marginal difference in the surge residuals at Visakhapatnam from the coupled and uncoupled model runs. It clearly indicates that the role of wave-induced setup at this location is insignificant, as seen in the TWE. In contrast, at Konada, the wave-induced setup
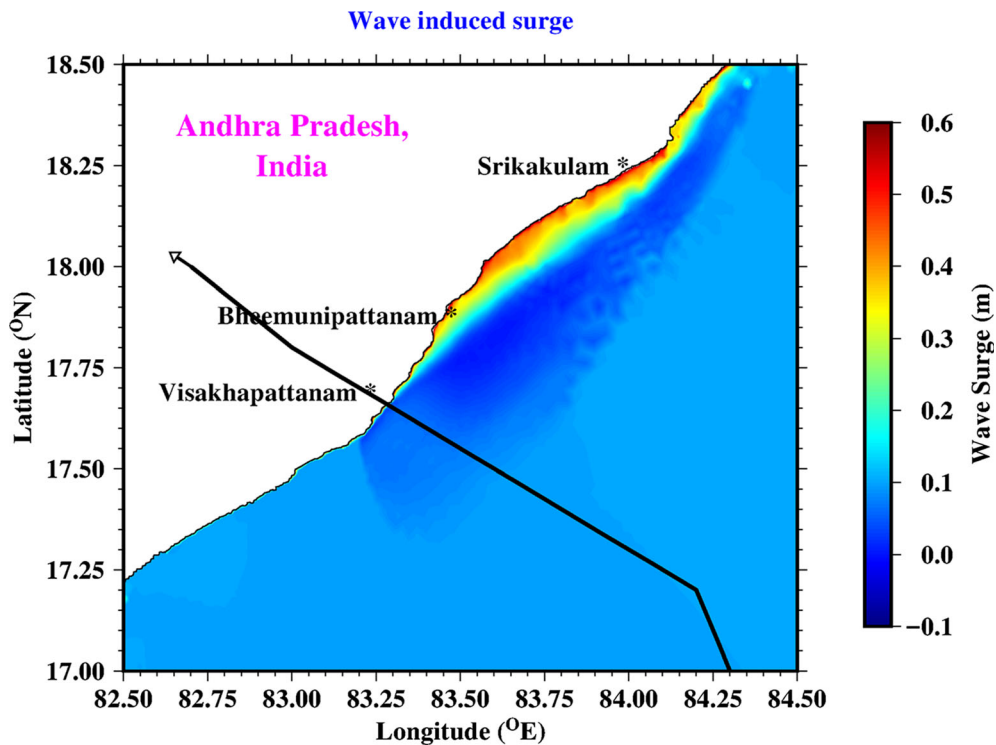

Figure 7
Spatial representation of wave-induced surge levels between Visakhapattanam and Srikakulam locations along the Andhra Pradesh coast. Black line with an arrow mark is the track of the cyclone)

Table 1

Comparison of uncoupled- and coupled-model-computed surge heights and inundation extents along the coastal region affected by Hudhud

Long	Lat	Surge (m)		Inundation extent (m)			Location name	District	State
		ADCIRC	ADCIRC + SWAN	ADCIRC	ADCIRC + SWAN	Observed			
84.009	18.246	1.50	2.04	405	405	–	Srikurmam	Srikakulam	Andhra Pradesh
83.249	17.630	1.13	1.44	214	214	–	Nadupuru	Vishakhapatnam	Andhra Pradesh
83.945	18.215	1.61	2.14	117	90	–	Mofusbandar	Srikakulam	Andhra Pradesh
83.627	18.046	2.17	2.65	110	140	150	Pathivada	Vizianagaram	Andhra Pradesh
83.830	18.161	1.73	2.29	112	132	–	Kuppili	Srikakulam	Andhra Pradesh
83.823	18.159	1.74	2.34	102	102	–	Kuppili	Srikakulam	Andhra Pradesh
83.800	18.149	1.81	2.31	89	80	–	Kuppili	Srikakulam	Andhra Pradesh
83.458	17.894	2.36	2.96	89	85	–	Bhimunipatnam	Vishakhapatnam	Andhra Pradesh
83.815	18.156	1.79	2.38	89	80	–	Kuppili	Srikakulam	Andhra Pradesh
83.665	18.077	2.05	2.56	90	90	80	Chintapalle	Srikakulam	Andhra Pradesh
83.358	17.752	1.73	2.19	84	84	–	ENDADA	Vishakhapatnam	Andhra Pradesh
83.938	18.211	1.65	2.17	80	100	150	Bontalakoduru	Srikakulam	Andhra Pradesh
83.672	18.082	1.91	2.44	78	90	100	Mentada	Srikakulam	Andhra Pradesh
83.303	17.691	1.44	2.01	78	80	–	Visakhapatnam	Vishakhapatnam	Andhra Pradesh
83.430	17.859	2.19	2.54	77	72	60	Nerallavalasa	Vishakhapatnam	Andhra Pradesh
83.700	18.098	2.07	2.56	73	110	100	Tekkali	Srikakulam	Andhra Pradesh
83.417	17.835	2.25	2.84	64	98	–	Kapuluppada	Visakhapatnam	Andhra Pradesh
83.566	18.000	2.35	2.85	61	70	–	Kongavanipalem	Vizianagaram	Andhra Pradesh
83.868	18.174	1.69	2.19	60	60	–	Koyyam	Srikakulam	Andhra Pradesh
83.960	18.221	1.35	1.90	54	70	–	Ippili	Srikakulam	Andhra Pradesh
83.721	18.110	2.00	2.50	53	108	120	Ramachandrapuram	Srikakulam	Andhra Pradesh
83.953	18.217	1.56	2.09	50	122	–	Mofusbandar	Srikakulam	Andhra Pradesh

Available records of observed inundation extent were also tabulated

increased the storm surge heights as the cyclone approached the landfall location, attributed to diverse features in the coastal geomorphology. The results reveal that the effect of wave-induced setup on TWE depends on the nearshore dynamics and coastal geomorphology. In addition, the effect of wave-induced setup is also governed by the width of the continental shelf. A recent study attempted by
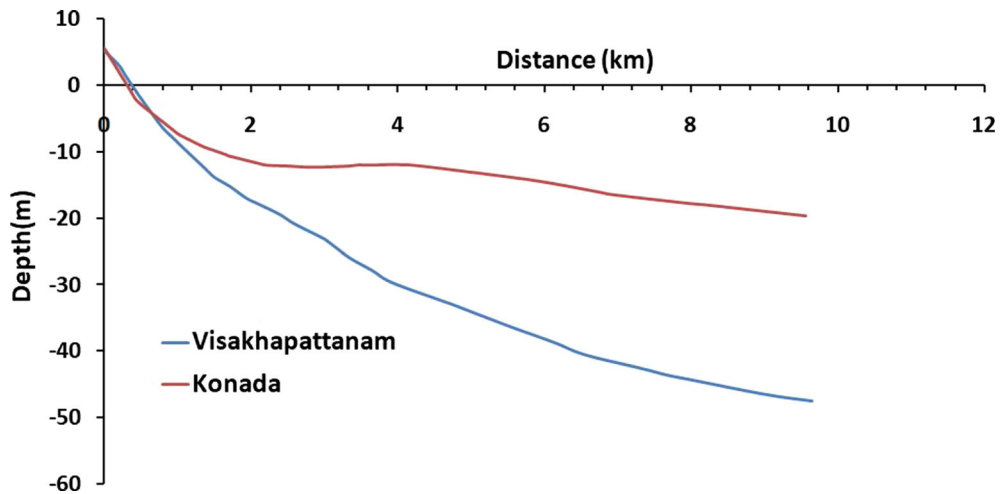
Figure 8
Bathymetric change towards off-shore at Visakhapattanam and Konada locations

Poulose and Rao (2017) reported on the influence of continental shelf geometry on the nonlinear interaction between storm surges, tides and wind waves based on an idealized experiment representing the west coast of India. Figure 8 shows the cross-shore bathymetry variation at Visakhapatnam and Konada locations. From this figure, it is very clear that the

cross-shore bottom profile is flat near Konada (with steepness 1:600) as compared with the location off Visakhapatnam (1:200). This is reflected in the uncoupled and coupled model simulations, indicating a reduction in the root mean square error (RMSE) from 0.30 to 0.18 m, respectively. Figure 10 shows the comparison of significant wave height between
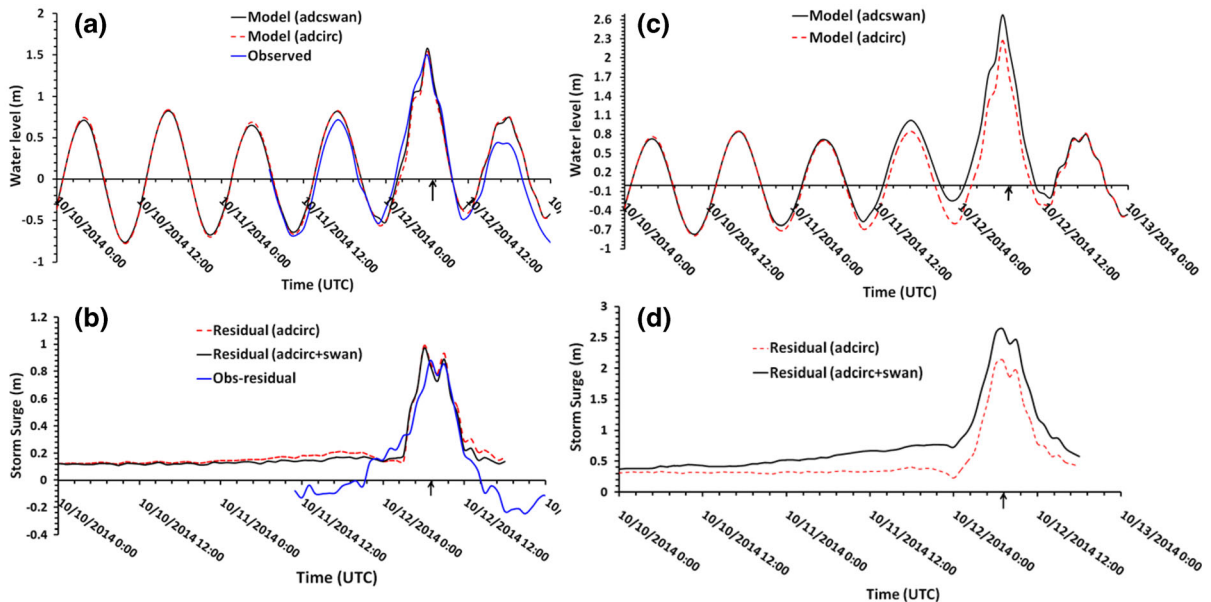

Figure 9
Validation of computed **a** water levels (includes tide), **b** surge residuals at Visakhapattanam. Depiction of **c** computed water levels (includes tide), **d** surge residuals at Konada (peak surge locations)
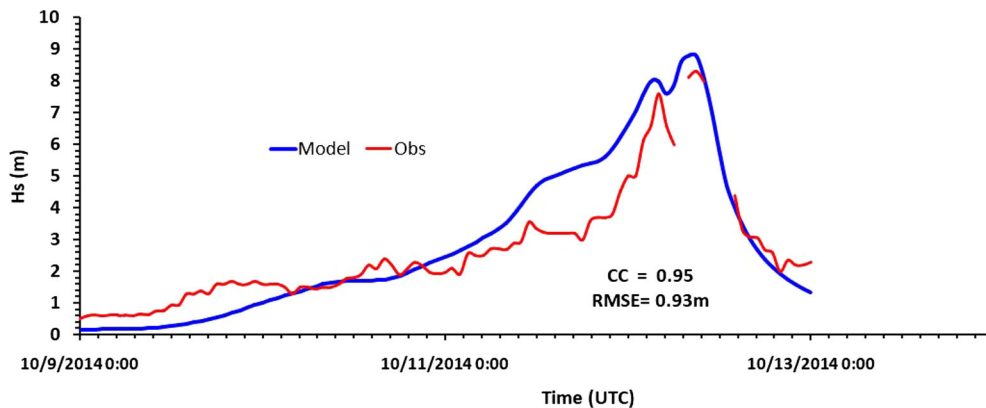
Figure 10
Validation of computed significant wave height at the Visakhapattanam wave rider buoy location

in situ observation and modeling. Significant wave height observations during Hudhud was obtained from the Visakhapatnam wave rider buoy. The time stamp of significant wave heights represented along the abscissa in Fig. 10 correspond to the duration when Hudhud intensified from a severe cyclonic storm (SCS, October 10, 2014; 0300 UTC) to a very severe cyclonic storm (VSCS, October 10, 2014; 0900 UTC). The modeled significant wave heights are in good agreement with the observed wave heights. This agreement is also statistically significant, as indicated by the high correlation coefficient (CC) of 0.95 and RMSE of 0.9 m.

4.2. Cyclone Phailin

Phailin was a very severe cyclonic storm that made landfall along the Odisha coast, India, on 12 October, 2013 and is regarded as the most intense cyclone after the Odisha super-cyclone (Kotal et al. 2015). Model simulation was carried out for 96 h since the cyclone developed over the open ocean. The track of Phailin is shown in Fig. 5. The coupled and uncoupled models computed the peak surge near the Ganjam (85.06°E, 19.37°N) location, Odisha. The storm surge computed with uncoupled model run was about 2.0 m, and the same using the coupled model was about 2.7 m, which shows the effect of wave radiation stress in the total water level elevation. Figure 11a, b illustrates the scenarios of storm surge and computed inundation extent by the uncoupled

and coupled model runs, respectively. Figure 11c, d is the enlarged version corresponding to Fig. 11a, b at the Anandpur (85.54°E, 19.70°N) location. Similarly, Fig. 11e, f is the magnified version corresponding to Fig. 11a, b, respectively, for the Ganjam location. It is very clear that the computed storm surge heights and inundation extents are higher at both the locations with the coupled model run, with a difference of about 0.6 m. The study signifies that the contribution from wave radiation stress was about 30% in the total water level elevation. The spatial distribution of wave-induced water levels is shown in Fig. 12. It is clear from this figure that the entire coastal stretch spanning from landfall point to Srikakulam is affected by wave setup with a peak value of about 0.6 m during this event. The dark blue shade in the figure corresponds to the wave set-down process. Table 2 lists the comparison of storm surge levels and corresponding inundation extent as computed by the coupled and uncoupled models at different locations during this extreme event. It is clear from Table 2 that the model-computed inundation extents were close to observations in the coupled model runs. Comparison of computed TWE and surge residuals against observed data off the Paradip location are shown in Fig. 13a, b, respectively. The overall comparison showed a very good match between model and observed surge residuals. Figure 13c, d shows the time evolution of TWE and surge residuals, respectively, at the location of peak surge (Ganjam) during Phailin. The arrow marked in the
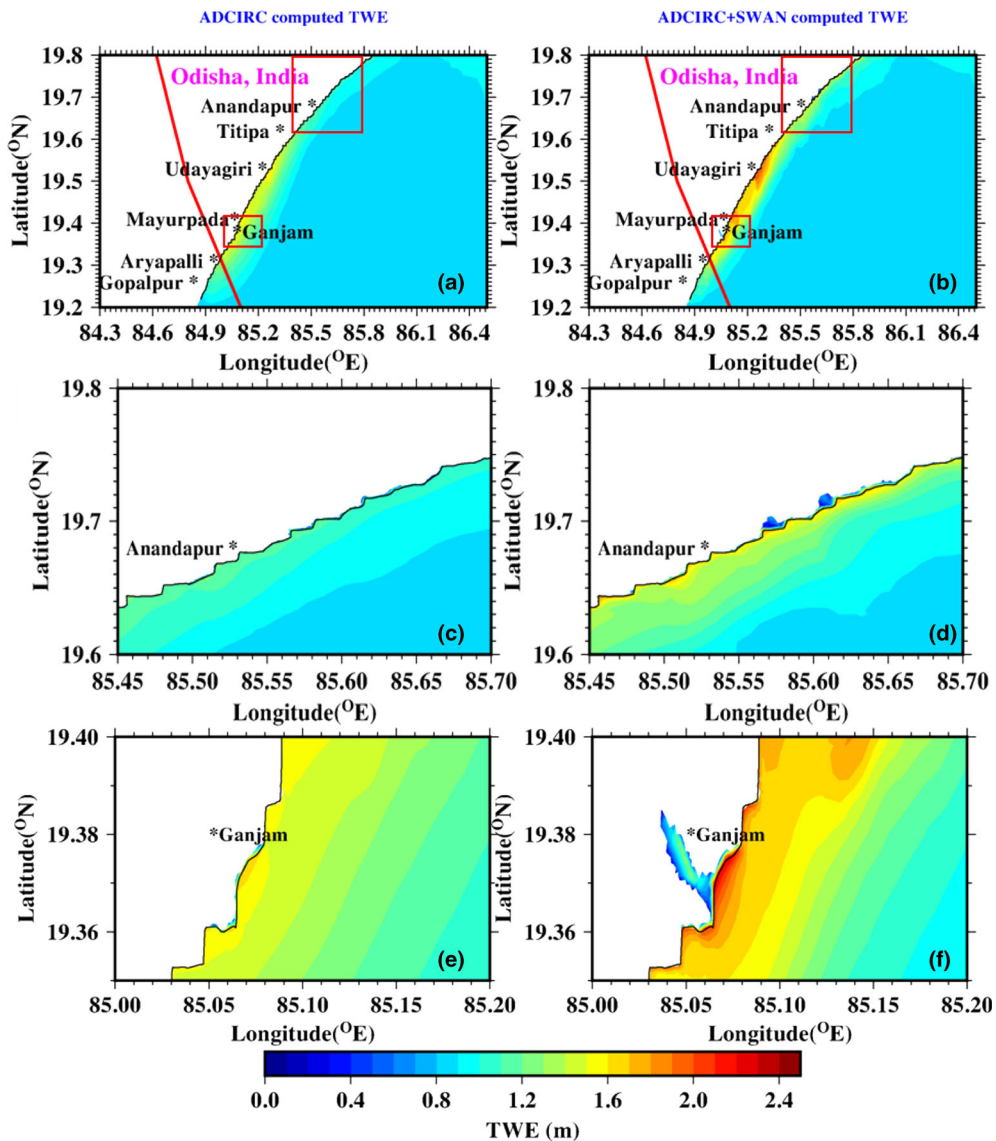
Figure 11
Spatial depiction of storm surge and computed inundation extents due to Phailin by **a** uncoupled, **b** coupled simulations. **c** Enlarged view of the red-colored box in **a** at the Anandpur location, **d** enlarged view of red-colored box in **b** at the Anandpur location, **e** enlarged view of the red-colored box in **a** at the Ganjam location and **f** enlarged view of the red-colored box in **b** at the Ganjam location. (TWE is total water elevation, and the red arrow indicates the cyclone track)

figure indicates the landfall time. As there are no observational data available near the peak storm surge location, only the modeled TWE and surge residuals are shown in Fig. 13c, d. Statistical measures of comparison between uncoupled and coupled model runs indicate reduced RMSE from 0.14 to 0.09 m, proving the robustness of the coupled model.

The dynamic characteristics of still water level elevation, the wave-induced setup and the set-down processes along coastal areas, especially during an approaching storm, have increasing effects that depend on the mutual interaction between waves, surges, currents and tides (Murty et al. 2014). For both the Hudhud and Phailin cases, the coupled
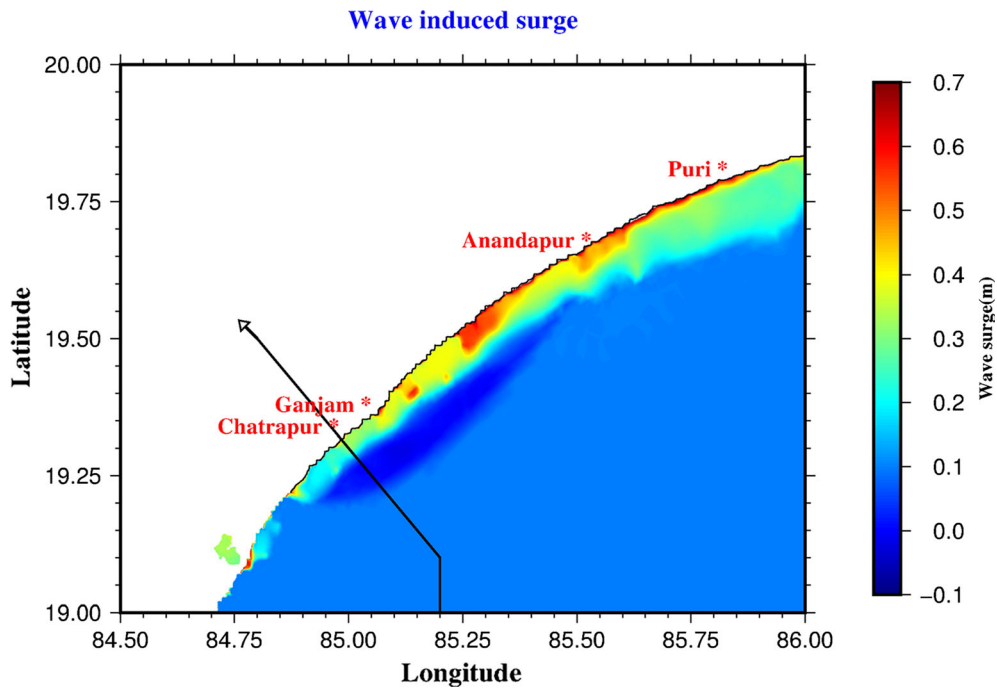
Wave induced surge

Figure 12
Spatial representation of wave-induced surge levels between Chatrapur and Puri locations along the Odisha coast (black line with arrow mark is the track of the cyclone)

model simulation that included the wave–surge–tide interaction component produced greater surge heights and inundation extents than the uncoupled simulation. In the case of Hudhud, though the surge heights are greater in the case for the coupled versus uncoupled run, there is no significant difference in the extent of inundation. However, in the case of Phailin, a significant difference is found in both the surge heights and the inundation extent between coupled and uncoupled simulations. It is well known that variations in local topographical features can affect the extent of inland inundation. The flat topography surrounding the Ganjam location, where the peak surge occurred during this event, contributes to the observed differences. On the other hand, for the Visakhapatnam location, where Hudhud made its landfall, has a steep topographical gradient, thereby resisting the inland penetration of storm surge that was higher. It is noted from the study that incorporation of wave-induced setup escalates the inundation distance as seen for the Phailin case which in turn depends on the coastal geomorphologic features. It is

also observed from this study that the inundation extent increased to a maximum by about 260 m and 50 m during the Phailin and Hudhud events, respectively. These observations are in line with the study reported by Wu et al. (2018). Figure 14 shows the comparison of significant wave height between observation and model output. Significant wave height data during Phailin was obtained from the Gopalpur wave rider buoy. The modeled significant wave heights are in good agreement with the observed significant wave heights. This agreement is also statistically significant, as indicated by the high CC of 0.96 and RMSE of 0.8 m.

5. Conclusions

Previous studies have shown that wave–current interactions can significantly influence coastal currents and water level elevations. From a global perspective, very few studies are available for other coastal regions, and there are no studies for the Indian

Table 2

Comparison of surge heights and inundation extents computed by uncoupled and coupled models along the coastal region affected by Phailin

Long (°)	Lat (°)	Surge (m)		Inundation extent (m)			Place name	District	State
		ADCIRC	ADCIRC + SWAN	ADCIRC	ADCIRC + SWAN	Observed			
85.062	19.366	2.1	2.8	110	392	110	Pallibanda	Ganjam	Odisha
85.579	19.695	1.08	1.52	76	392		Manikapatna	Puri	Odisha
84.915	19.264	0.99	1.08	110	152		Haripur	Ganjam	Odisha
85.411	19.617	1.20	1.71	22	185		Janhikuda	Puri	Odisha
85.093	19.404	1.62	2.17	50	215	195		Ganjam	Odisha
85.290	19.550	1.58	2.11	–	132		Nabaeatarea	Puri	Odisha
85.571	19.692	1.06	1.52	23	183		Manikapatna	Puri	Odisha
85.404	19.612	1.08	1.62	–	130		Biripadar	Puri	Odisha
85.511	19.659	1.16	1.61	–	110		Sipakuda	Puri	Odisha
85.057	19.362	1.11	1.92	–	100	70		Ganjam	Odisha
85.309	19.560	1.54	1.99	–	80		Ora	Puri	Odisha
85.343	19.585	1.41	2.07	22	70		Jamuna	Puri	Odisha
84.895	19.239	1.12	1.23	77	77		Hatipada	Ganjam	Odisha
85.397	19.608	1.27	1.86	77	77		Biripadar	Puri	Odisha
85.277	19.534	1.50	2.01	71	71		Fatepur	Puri	Odisha
85.840	19.193	0.76	1.11	–	80	60		Ganjam	Odisha
85.112	19.417	1.67	2.07	68	68		Padagadajhatipadar	Ganjam	Odisha
85.443	19.634	1.11	1.49	54	54		Berhampur	Puri	Odisha

Available records of observed inundation extent were also tabulated
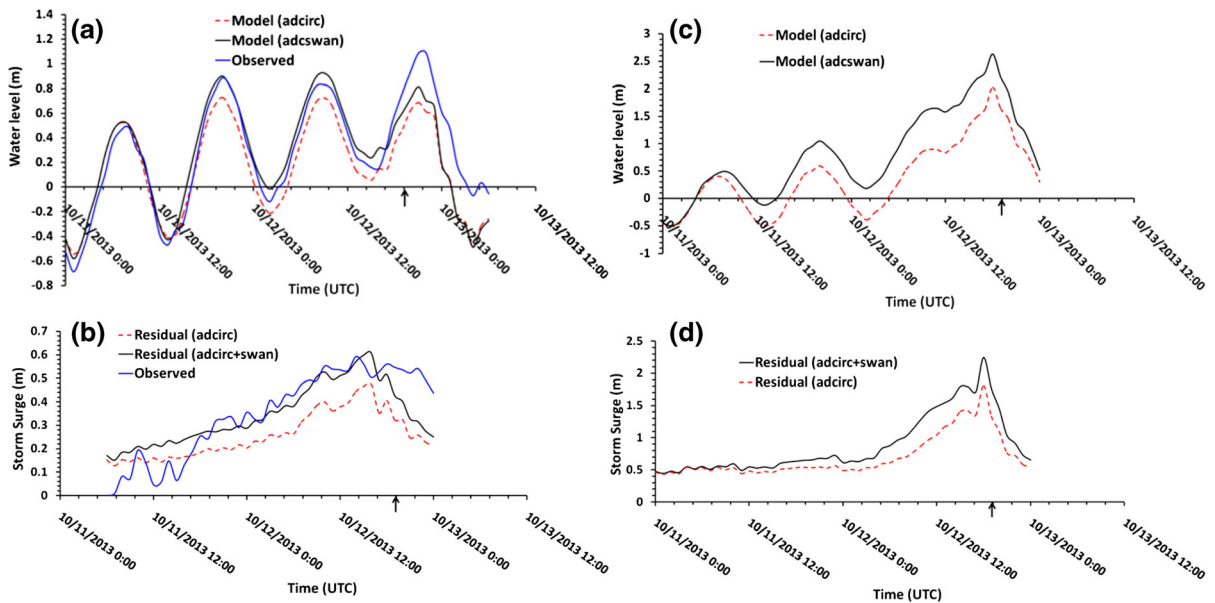

Figure 13
Validation of computed **a** water levels (includes tide), **b** surge residuals at Paradip. Depiction of **c** computed water levels (includes tide), **d** surge residuals at Ganjam (peak surge locations)

coast that examined the overall contribution of wave setup on storm surge-induced coastal inundation. The present study is an application of uncoupled ADCIRC and a coupled ADCIRC + SWAN models to simulate storm surges and associated coastal inundation for very severe cyclonic storms Hudhud and Phailin
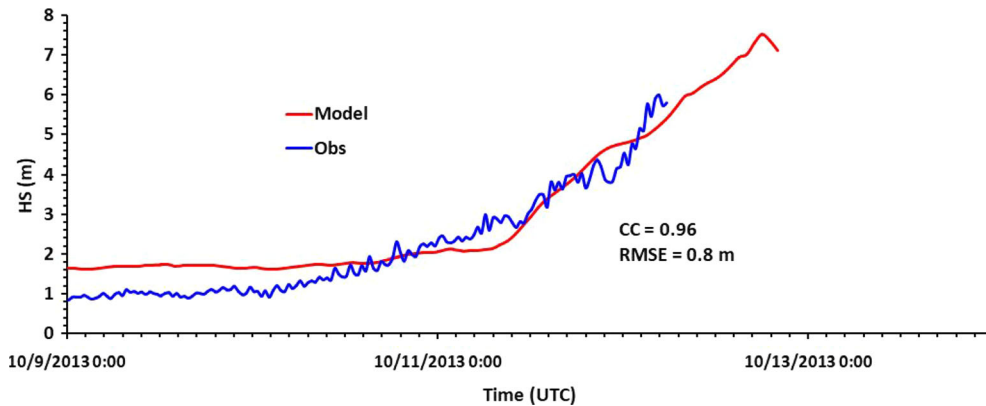
Figure 14
Validation of computed significant wave height at the Visakhapattanam wave rider buoy location

cases. To explore the influence of surface gravity waves on storm surge and coastal inundation, a series of experiments were conducted. While the interaction between tide and surge and their mutual effects during extreme events such as tropical storms have been studied previously for the ECI, a detailed investigation of the interaction mechanism between tide, wave and surge, and the manner in which it affects storm surge heights and coastal inundation, has been lacking. The inclusion of wave radiation stress is very critical for improving model performance and for better representation of computed storm surge heights (Araújo et al. 2011). In the present study, the contribution of wave radiation stress and its influence on surge heights and coastal inundation was investigated during the recent very severe cyclonic storms Hudhud and Phailin that made landfall along the ECI. A finite element-based unstructured model, ADCIRC, in a stand-alone mode, and the ADCIRC + SWAN model (coupled mode) were used to perform the simulations. Meteorological forcing fields were generated using the Holland-2010 formulation to force the storm surge model. Results showed that the wave-induced radiation stresses contributed an approximately 20% (30%) increase in surge heights at the peak surge locations during Hudhud (Phailin) events, supported by Dietrich et al. (2011) and Sheng et al. (2010). From the time-series distribution for the Hudhud case, it is evident that the wave setup effect on total water elevation off the Visakhapatnam location is less significant or negligible. The results

also indicate that the coupled model simulation showed an increase in the inundation extent along the Odisha coast during the Phailin event. On the other hand, there was no significant difference observed in the inundation extent with and without wave setup for the Hudhud simulation, indicating that local near-shore topography plays a significant role in governing the horizontal extent of inundation even though the surge heights are large. The study further signifies that the effect of wave–current interaction must necessarily be taken into account in storm surge calculations and, more importantly, in better representation of the inundation extent. It brings to light the importance of flat topography in modulating the extent of inundation and the role of wave radiation stress in hydrodynamic modeling. Based on this study, it is clear that the coupled modeling system performed significantly better, proving its usefulness for real-time forecasting of storm surge and associated flooding.

Publisher's Note Springer Nature remains neutral with regard to jurisdictional claims in published maps and institutional affiliations.

REFERENCES

Arora, C., & Bhaskaran, P. K. (2012). Parameterization of bottom friction under combined wave-tide action in the Hooghly estuary, India. *Ocean Engineering, 43,* 43–55.

Arora, C., Kumar, B. P., Jain, I., Bhar, A., & Narayana, A. C. (2010). Bottom boundary layer characteristics in the Hooghly estuary under combined wave-current action. *Marine Geodesy, 33*(2), 261–281.

Bao, J. W., Wilczak, J. M., Choi, J. K., & Kantha, L. H. (2000). Numerical simulations of air-sea interaction under high wind conditions using a coupled model: A study of hurricane development. *Monthly Weather Review*, *128*, 2190–2210.

Bhaskaran, P. K., Gayathri, R., Murty, P. L. N., Subba Reddy, B., & Sen, D. (2014). A numerical study of coastal inundation and its validation for Thane cyclone in the Bay of Bengal. *Coastal Engineering, 83,* 108–118.

Bhaskaran, P. K., Nayak, S., Bonthu, S. R., Murty, P. L. N., & Sen, D. (2013). Performance and validation of a coupled parallel ADCIRC–SWAN model for THANE cyclone in the Bay of Bengal. *Environmental Fluid Mechanics, 13*(6), 601–623.

Blain, C. A., Westerink, J. J., & Luettich, R. A. (1998). Grid convergence studies for the prediction of hurricane storm surge. *International Journal for Numerical Methods in Fluids, 26,* 369–401.

Booij, N., Ris, R. C., & Holthuijsen, L. H. (1999). A third-generation wave model for coastal regions, part-I model descriptions and validation. *Journal of Geophysical Research, 104*(C4), 7649–7666.

Brown, J. M., Bolaños, R., & Wolf, J. (2011). Impact assessment of advanced coupling features in a tide-surge-wave model, POLCOMS-WAM, in a shallow water application. *Journal of Marine Systems, 87*(1), 13–24.

Brown, J. M., & Wolf, J. (2009). Coupled wave and surge modelling for the eastern Irish Sea and implications for model wind-stress. *Continental Shelf Research, 29*(10), 1329–1342.

Bung, H. C., Byung, I. M., Kyeong, O. K., & Jin, H. Y. (2013). Wave-tide-surge coupled simulation for typhoon Maemi. *China Ocean Engineering, 27*(2), 141–158.

Dietrich JC (2010) Development and Application of coupled Hurricane wave and surge models for Southern Louisiana. (Ph.D Thesis) University of Notre Dame, p. 337.

Dietrich, J. C., Zijlema, M., Westerink, J. J., Holthuijsen, L. H., Dawson, C. N., Luettich, R. A., Jr., et al. (2011). Modeling hurricane waves and storm surge using integrally-coupled, scalable computations. *Coastal Engineering, 58,* 45–65.

Donelan, M. A., Dobson, F. W., Smith, S. D., & Anderson, R. J. (1993). On the dependence of sea surface roughness on wave development. *Journal of Physical Oceanography, 23,* 2143–2149.

Dube, S. K., Chittibabu, P., Rao, A. D., Sinha, P. C., & Murty, T. S. (2000). Extreme sea levels associated with severe tropical cyclones hitting Orissa coast of India. *Marine Geodesy, 23,* 75–90.

Dube, S. K., Rao, A. D., Sinha, P. C., Murty, T. S., & Bahulayan, N. (1997). Storm surge in the Bay of Bengal and Arabian Sea: The problem and its prediction. *Mausam, 48*(2), 283–304.

Ferrarin, C., Roland, A., Bajo, M., Umgiesser, G., Cucco, A., Davolio, S., et al. (2013). Tide-surge-wave modelling and forecasting in the Mediterranean Sea with focus on the Italian coast. *Ocean Modelling, 61,* 38–48.

Fleming, J., Fulcher, C., Luettich, R. A., Estrade, B., Allen, G., & Winer, H. (2008). A real time storm surge forecasting system using ADCIRC. *Estuarine and Coastal Modeling, 2008,* 893–912.

Garratt, J. R. (1977). Review of drag coefficients over oceans and continents. *Monthly Weather Review, 105,* 915–929.

Gayathri, R., Murty, P. L. N., Bhaskaran, P. K., & Srinivasa Kumar, T. (2016). A numerical study of hypothetical storm surge and coastal inundation for AILA cyclone in the Bay of Bengal. *Environmental Fluid Mechanics, 16*(2), 429–452.

Hasselmann, S., Hasselmann, K., Allender, J. H., & Barnett, T. P. (1985). Computations and parameterizations of the nonlinear energy transfer in a gravity wave spectrum. Part II: parameterizations of the nonlinear transfer for application in wave models. *Journal of Physical Oceanography, 15*(11), 1378–1391.

Holland, G. J. (1980). An analytic model of the wind and pressure profiles in hurricanes. *Monthly Weather Review*, *108*, 1212–1218.

Holland, G. J., James, B. I., & Fritz, Angela. (2010). A revised model for radial profiles of hurricane winds. *American Meteorological Society*. https://doi.org/10.1175/2010MWR3317.1.

Holthuijsen, L. H. (2007). *Waves in oceanic and coastal waters*. New York: Cambridge University Press. https://doi.org/10.1017/CBO978051161853.

Horsburgh, K. J., & Wilson, C. (2007). Tide-surge interaction and its role in the distribution of surge residuals in the North Sea. *Journal of Geophysical Research, 112,* C08003.

Houston, S. H., Shaffer, W. A., Powell, M. D., & Chen, J. (1999). Comparisons of HRD and SLOSH surface wind fields in hurricanes: implications for storm surge modeling. *Weather Forecast, 14,* 671–686.

Hwang, P. A. (2018). High-wind drag coefficient and whitecap coverage derived from microwave radiometer observations in tropical cyclones. *Journal of Physical Oceanography, 48,* 2221–2232.

Janssen, P. A. E. M. (1992). Experimental evidence of the effect of surface waves on the airflow. *Journal of Physical Oceanography*, *22*, 1600–1604.

Kotal, S. D., Bhattacharya, S. K., & Rama Rao, Y. V. (2015). NWP report on cyclonic storms over the north Indian Ocean during 2014, IMD.

Le Provost, C., Lyard, F., Molines, J. M., Genco, M. L., & Rabilloud, F. (1998). A hydrodynamic ocean tide model improved by assimilating a satellite altimeter-derived data set. *Journal of Geophysical Research*, *103*, 5513–5529.

Longuet-Higgins, M. S., & Stewart, R. W. (1960). Changes in the form of short gravity waves on long waves and tidal currents. *Journal of Fluid Mechanics*, *8*, 565–583.

Longuet-Higgins, M. S., & Stewart, R. W. (1962). Radiation stress and mass transport in gravity waves, with application to "surf-beats". *Journal of Fluid Mechanics*, *13*, 481–504.

Luettich, R.A. Jr., Westerink, J.J., Scheffner, N.W. (1992). ADCIRC: An advanced three dimensional circulation model for shelves coasts and estuaries, report 1: Theory and methodology

of ADCIRC-2DDI and ADCIRC-3DL. Dredging Research Program Technical Report DRP-92-6, US Army Engineers Waterways Experiment Station, Vicksburg, MS, USA, p. 137.

Madsen, O.S., Poon, Y.K., Graber, H.C. (1988). Spectral wave attenuation by bottom friction—theory. In: Proceedings of the 21st ASCE Coastal Eng. Conf., pp. 492–504.

Mastenbroek, C., Burgers, G., & Janssen, P. A. E. M. (1993). The dynamical coupling of a wave model and a storm surge model through the atmospheric boundary layer. *Journal of Physical Oceanography*, 23, 1856–1866.

Mellor, G. L. (2003). The three-dimensional current and surface wave equations. *Journal of Physical Oceanography*, 33, 1978–1989.

Murty, P. L. N., Bhaskaran, P. K., Gayathri, R., Sahoo, B., Kumar, T. S., & SubbaReddy, B. (2016). Numerical study of coastal hydrodynamics using a coupled model for Hudhud cyclone in the Bay of Bengal. *Estuarine, Coastal Shelf Science*, 183, 13–27.

Murty, T. S., Flather, R. A., & Henry, R. F. (1986). The storm surge problem in the Bay of Bengal. *Progress in Oceanography, 16,* 195–233.

Murty, P. L. N., Sandhya, K. G., Bhaskaran, P. K., Felix, J., Gayathri, R., Balakrishnan Nair, T. M., et al. (2014). A coupled hydrodynamic modeling system for PHAILIN cyclone in the Bay of Bengal. *Coastal Engineering, 93*(2014), 71–81.

Nayak, S., & Bhaskaran, P. K. (2013). Coastal vulnerability due to extreme waves at Kalpakkam based on historical tropical cyclones in the Bay of Bengal. *International Journal of Climatology.* https://doi.org/10.1002/joc.3776.

Nayak, S., Bhaskaran, P. K., & Venkatesan, R. (2012). Near-shore wave induced setup along Kalpakkam coast during an extreme cyclone event in the Bay of Bengal. *Ocean Engieering, 55,* 52–61.

Ozer, J., Padilla-Hernandez, R., Monbaliu, J., Alvarez Fanjul, E., CarreteroAlbiach, J. C., Osuna, P., et al. (2000). A coupling module for tides, surges and waves. *Coastal Engineering, 41,* 95–124.

Poulose, J., & Rao, A. D. (2017). Bhaskaran PK (2017) Role of continental shelf on non-linear interaction of storm surges, tides and wind waves: An idealized study representing the west coast of India, Estuarine. *Coastal and Shelf Science.* https://doi.org/10.1016/j.ecss.2017.06.007.

Powell, M. D., & Reinhold, T. A. (2007). Tropical cyclone destructive potential by integrated kinetic energy. *Bulletin of the American Meteorological Society*, 88, 513–526.

Prandle, D., & Wolf, J. (1978). The interaction of surge and tide in the North Sea and River Thames. *Geophysical Journal of the Royal Astronomical Society*, 55, 203–216.

Rajesh Kumar, R., Prasad Kumar, B., Satyanarayana, A. N. V., BalaSubrahmanyam, D., Rao, A. D., & Dube, S. K. (2009). Parameterization of sea surface drag under varying sea state and its dependence on wave age. *Natural Hazards, 49*(2), 187–197.

Rao, A. D., Dube, S. K., & Chittibabu, P. (1994). Finite difference technique applied to the simulation of surges and currents around Sri Lanka and Southern Indian Peninsula. *Computational Fluid Dynamics, 3,* 71–77.

Rao, A. D., Indu, J., Ramana Murthy, M. V., Murty, T. S., & Dube, S. K. (2009). Impact of cyclonic wind field on interaction of surge-wave computations using finite-element and finite-difference models. *Natural Hazards, 49,* 225–239.

Rao, A. D., Murty, P. L. N., Jain, I., Kankara, R. S., Dube, S. K., & Murty, T. S. (2012). *Simulation of water levels and extent of coastal inundation due to a cyclonic storm along the east coast of India*. Nat: Hazards. https://doi.org/10.1007/s11069-012-0193-6.

Roland, A., Cucco, A., Ferrarin, C., Hsu, T. W., Liau, J. M., Ou, S. H., et al. (2009). On the development and verification of a 2d coupled wave-current model on unstructured meshes. *Journal of Marine Systems, 78*(Supplement), S244–S254.

Sheng, Y. P., Yanfeng, Z., & Vladimir Paramygin, A. (2010). Simulation of storm surge, wave, and coastal inundation in the North eastern Gulf of Mexico region during Hurricane Ivan in 2004. *Ocean Modelling, 35*(2010), 314–331.

Smita, P., & Rao, A. D. (2018). An improved cyclonic wind distribution for computation of storm surges. *Natural Hazards, 92,* 93–112.

Smith, S. D., Anderson, R. J., Oost, W. A., Kraan, C., Maat, N., et al. (1992). Sea surface wind stress and drag coefficients: The HEXOS results. *Boundary-Layer Meteorology, 60,* 109–142.

Srinivasa, K. T., Murty, P. L. N., Pradeep, K. M., Krishna, K. M., Padmanabham, J., Kiran, K. N., et al. (2015). Modeling storm surge and its associated inland inundation extent due to very severe cyclonic storm Phailin. *Marine Geodesy, 38,* 345–360.

Vongvisessomjai, S., & Rojanakamthorn, S. (1989). Interaction of tide and river flow. *Journal of Waterway, Port, Coastal, and Ocean Engineering, 115*(1), 86–103.

Welsh, D. J. S., Bedford, K. W., Wang, R., & Sadayappan, P. (2000). *A parallel-processing coupled wave/current/sediment transport model*. Technical Report ERDC MSRC/PET TR/00-20. Vicksburg, MS: U.S. Army Engineer Research and Development Center.

Wolf, J. (2009). Coastal flooding: impacts of coupled wave-surge-tide models. *Natural Hazards, 49*(2), 241–260.

Wu, J. (1982). Wind-stress coefficients over sea surface from breeze to hurricane. *Journal of Geophysical Research: Oceans, 87,* 9704–9706.

Wu, G., Shi, F., Kirby, J. T., Liang, B., & Shi, J. (2018). Modeling wave effects on storm surge and coastal inundation. *Coastal Engineering.* https://doi.org/10.1016/j.coastaleng.2018.08.011.

Xie, L., Wu, K., Pietrafesa, L. J., & Zhang, C. (2001). A numerical study of wave-current interaction through surface and bottom stresses: Wind-driven circulation in the South Atlantic Bight under uniform winds. *Journal of Geophysical Research*, 106, 16841–16855.

Xie, L., Pietrafesa, L. J., & Peng, M. (2004). Incorporation of a mass-conserving inundation scheme into a three dimensional storm surge model. *Journal of Coastal Research*, 20, 1209–1223.

Zachry, B. C., Schroeder, J. L., Kennedy, A. B., Westerink, J. J., & Letchford, C. W. (2013). A case study of nearshore drag coefficient behavior during Hurricane Ike (2008). *Journal of Applied Meteorology and Climatology, 52,* 2139–2146.

Ziegler, C.K., Bales, J.D., Robbins, J.C., Blumberg, A.F. (1993). A comparative analysis of estuarine circulation simulations using laterally averaged and vertically averaged hydrodynamic models. In M. Spaulding, K. Bedford, A. Blumberg, R. Cheng, C. Swanson (Eds.) Proceedings of the 3rd International Conf. On Estuarine and Coastal Modeling. III. ASCE, New York, pp. 447–460.

Zijlema, M. (2010). Computation of wind wave spectra in coastal waters with SWAN on unstructured grids. *Coastal Engineering, 57,* 267–277.